Ripple-Trapped Loss of Neutral-Beam-Injected Fast Ions in JT-60U

K. Tobita, K. Tani, Y. Neyatani, A. A. E. van Blokland, S. Miura, T. Fujita, H. Takeuchi, T. Nishitani, M. Matsuoka, and S. Takechi[a]

Japan Atomic Energy Research Institute, Naka Fusion Research Establishment, Naka-machi, Naka-gun, Ibaraki, 311-01 Japan

(Received 28 February 1992)

Toroidal field ripple loss of neutral-beam-injected fast ions is measured from the heat load on the first wall in JT-60U. The heat load is localized in both toroidal and poloidal directions and increases with both ripple size and safety factor. The overall measured ripple loss is in good agreement with an orbit-following Monte Carlo calculation. Nevertheless, there is a small difference between the experimental and the calculated location of the maximum heat load, which suggests that the radial electric field shifts the impinging points of ripple-trapped ions on the first wall.

PACS numbers: 52.50.Gj, 52.55.Fa

The effects of toroidal field (TF) ripple on plasma confinement and transport have been investigated for the past several decades [1-3]. Compared with the number of theoretical and computational works, there have not been many experiments performed on the TF ripple. The ISX-B 9 vs 18 TF coil experiment [4] demonstrated for the first time adverse effects of the TF ripple, such as an enhancement of the ion thermal conductivity, fast-ion loss, and ripple damping of beam-induced toroidal plasma rotation. Recently, fast-ion behavior related to the TF ripple has been investigated in Tore Supra [5], JET [6], and JT-60U [7]. Stochastic ripple diffusion [8], which may play an important role in nonprompt alpha particle loss in a burning plasma, has been identified in TFTR [9]. One of the major problems of the TF ripple is the resulting localized heat deposition on the first wall [10]. In order to evaluate the heat deposition profile, several simulation codes have been developed to avoid the difficulties involved in an analytic treatment of the problem. In spite of the usefulness of the simulation codes for the problem, concerns about the reliability of the codes still remain, because of the complexity of the problem and the extremely time-consuming computations. Therefore, a quantitative comparison between experiment and calculation is the prime issue regarding ripple-induced fast-ion loss. Fast-ion ripple loss arises from two major processes: ripple-trapped loss and banana drift loss. The first quantitative measurements on ripple-trapped loss were performed in TFR [11], and it was reported that many experimental features were consistent with the calculations, but the observed ripple loss was twice as large as the calculated one.

This Letter describes the experiments on the ripple-trapped loss of nearly perpendicularly injected fast ions in JT-60U and shows a comparison between the experimental data and orbit-following Monte Carlo (OFMC) calculations [12]. Contrary to the TFR experiments, the present experiment agrees well with the prediction of the OFMC code. Finally, the effect of the radial electric field, which can weaken the peaking of the localized heat deposition of alpha particles on the first wall in a fusion reactor [13], is discussed. The results presented enhance the understanding of single-particle behavior of fast ions in nonaxisymmetric magnetic fields. It should be noted that stochastic ripple diffusion does not occur in our case because of the small banana width of the fast ions. Another importance of this work is that the quantitative agreement in fast-ion loss suggests nonanomalous transport and classical slowing down of energetic ions, which is in contrast with the well-known anomaly of ion thermal transport.

JT-60U is a tokamak with a major radius $R_0 = 3.4$ m, and an average minor radius $a = 0.9$ m. Its toroidal field is produced by eighteen circular coils and the toroidal field ripple δ [$\equiv (B_{max} - B_{min})/(B_{max} + B_{min})$] goes up to 2.2% at the outer edge of a full-size plasma. The toroidal ripple distribution is illustrated in Fig. 1. The experiments were performed under the following plasma conditions: current $I_P = 1.0$-4.0 MA, toroidal field $B_T = 2.0$-4.0 T, and $\delta = (0.2$-$2.0)\%$. The neutral-beam-injection (NBI) systems were operated with 10-18 MW nearly perpendicular injection (D^0, 80-90 keV). The tangency radius of the beam lines R_{tan}, which is defined as $R_{tan} = \eta R$ (where η and R denote the pitch angle of an

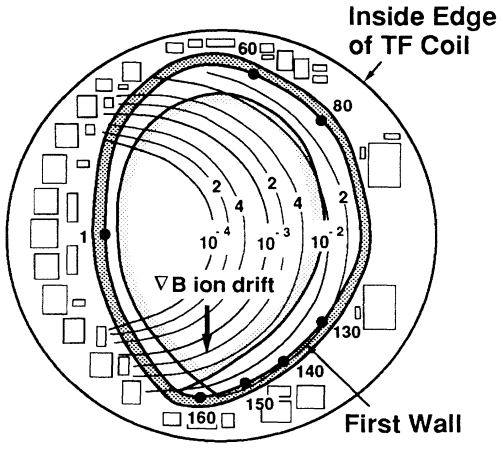

FIG. 1. Poloidal cross section of JT-60U plasma and the toroidal ripple distribution. Also shown are the poloidal position numbers of the first wall.

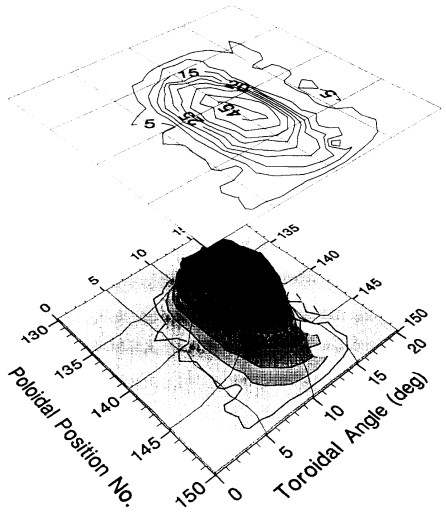

FIG. 2. Two-dimensional distribution of the heat deposition on the first wall. The TF coils are located at the toroidal angles of 0° and 20°. The heat flux peaks just between the TF coils. The magnitude of the heat flux is expressed in units of W/cm^2.

injected ion and the major radius where the fast ion is born, respectively), is 0.75 m. The power fraction of the NBI sources is $E:E_{1/2}:E_{1/3}=78\%:15\%:7\%$. Throughout the experiments, B_T and I_P were directed clockwise and hence the ion ∇B drift direction is oriented downward.

In these experiments we concentrated on the thermal measurements of the heat deposition on the first wall, which enabled straightforward measurements of ripple loss with good spatial resolution. The heat deposition was measured by thermocouples (TC) mounted on the wall and a fast infrared TV (IRTV) camera viewing the wall. The thermocouples consist of toroidal-poloidal TC arrays which cross near the heat spot due to fast-ion ripple loss. The only disadvantage of these thermal measurements is that they give no information on the physical origin of the heat deposition. To prove that the observed heat deposition was due to ripple loss, we considered multiple evidence like (i) the localization of heat deposition on the ∇B ion drift side, (ii) the increase in heat flux with ripple size, and (iii) the increase in heat flux with safety factor. The experimental observations described below indicate that the measured heat flux is attributed to ripple-lost fast ions.

Figure 2 shows the two-dimensional heat flux on the first wall measured by the IRTV. Here, the TF coils are located at toroidal angles of 0° and 20°, where the toroidal angle is taken in the direction of I_P and B_T. For convenience, we introduce the poloidal position (PP) numbers as shown in Fig. 1. Figure 2 indicates that the heat load is localized in both toroidal and poloidal directions: The heat flux peaks just between two TF coils on the ∇B ion drift side.

By changing the plasma size and position, we obtained

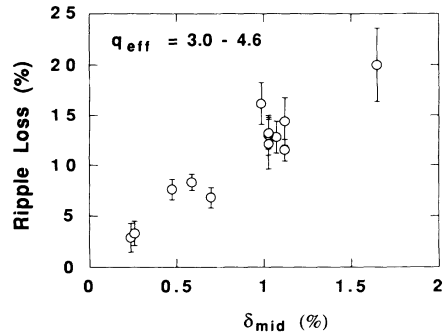

FIG. 3. Experimental ripple-loss fraction as a function of ripple size on the midplane δ_{mid}.

a relation between the ripple-loss fraction and the ripple magnitude δ_{mid}, where δ_{mid} denotes the toroidal ripple on the outermost magnetic surface on the midplane. As plotted in Fig. 3, the ripple-loss fraction increases with ripple size. Here, the ripple-loss fraction is defined as the ratio of the total ripple-loss power to the NBI power. The total ripple-loss power is estimated by assuming toroidal periodicity of the heat spot. This assumption is reasonable because, owing to toroidal precession, fast ions circumnavigate the torus several times before they become ripple trapped. Radiation and charge exchange (CX) losses can also be part of the heat deposition on the wall. We estimated the loss power due to these processes from the temperature rise of the first wall near the TF coils and corrected for their contribution. The error bars shown in the figure are mainly determined from the error in the estimation of radiation and CX loss power.

Ripple wells are formed in the region where the effective ripple well parameter α^* $[\equiv(\partial\bar{B}/\partial l)/(\partial\tilde{B}/\partial l)]$ satisfies $|\alpha^*|<1$, where we express the toroidal magnetic field as $B_\phi(r,\theta,\phi)=\bar{B}(r,\theta)+\tilde{B}(r,\theta)\cos N\phi$. Here, $\bar{B}$, $\tilde{B}$, θ, and ϕ stand for the axisymmetric and nonaxisymmetric components of the toroidal magnetic field, the poloidal angle, and the toroidal angle, respectively, and N is the number of TF coils. For a plasma with circular cross section, the ripple-trapping condition can be simplified to $|\alpha^*|=r|\sin\theta|/Nq\delta<1$ [1]. As expected from this condition, the ripple-trapping region extends with q. The poloidal distribution of the heat load is shown for different values of the effective safety factor [14] q_{eff} in Fig. 4. Here, the q_{eff} scan is performed by changing I_P. The heat deposition increases with q_{eff} because of the expansion of the ripple-trapping region with q_{eff}.

The above characteristics of the observed heat flux give evidence of fast-ion ripple loss. An important question on ripple loss is whether available computations predict the ripple loss quantitatively or not. Next we compare the experimental data with simulations by an OFMC code.

The OFMC code consists of four parts: (i) calculation of the ionization of the neutral-beam atoms, (ii) simulation of Coulomb collisions, (iii) calculation of the

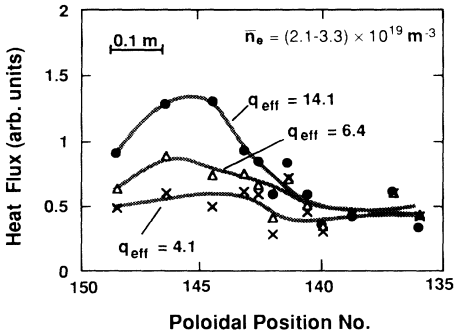

FIG. 4. The poloidal heat flux distribution for different values of q_{eff}. The heat deposition increases with q_{eff} because of the expansion of the ripple-trapping region.

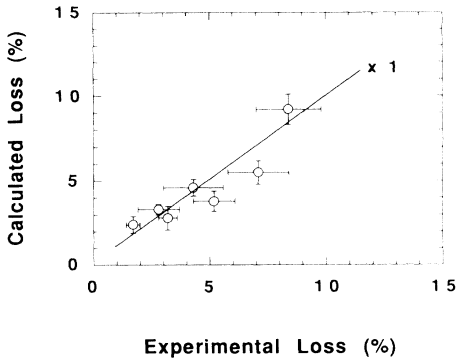

FIG. 5. Comparison of the experimental and calculated ripple-trapped loss fraction.

guiding-center orbit in nonaxisymmetric magnetic fields, and (iv) simulation of charge-exchange reactions of fast ions and reionization of the resultant neutrals. Of the above four parts, (i), (ii), and (iv) are solved using Monte Carlo techniques. In the code, fast ions produced by ionization of injected neutral beams are launched from their birth points and are followed until all of them are thermalized or lost to the first wall. The code does not include the radial electric field in the orbit calculation.

The comparison between the experiments and the OFMC calculations of the ripple-trapped loss is shown in Fig. 5. Good agreement between both is seen. Here, discharge parameters for the plotted data are $I_P = 2.5\text{-}4.0$ MA, $B_T = 4.0$ T, $q_{eff} = 2.9\text{-}4.7$, $\delta_{mid} = (0.2\text{-}0.5)\%$, and line-averaged electron density $\bar{n}_e = (2.5\text{-}4.5) \times 10^{19}$ m^{-3}. The error in the computation is attributed to the statistical error caused by the finite number of test particles used in the Monte Carlo calculations. These results indicate that the OFMC code predicts the ripple-trapped loss quantitatively.

A comparison between the experiment and the computation of the heat flux profiles on the first wall is done for a specific shot as shown in Fig. 6. The experimental and the simulated heat fluxes are represented by solid circles and dashed lines, respectively. We compare the toroidal and poloidal heat flux distributions by traversing the peaks, because there is a small difference in the position of the peak heat load between the experiment and the calculation. Discharge conditions for this shot were $I_P = 4.0$ MA, $B_T = 4.0$ T, $q_{eff} = 2.9$, NBI power $P_{NB} = 10.7$ MW, beam energy $E_b = 90$ keV, $\bar{n}_e = 2.3 \times 10^{19}$ m^{-3}, and the central ion and electron temperatures were 4.1 and 2.7 keV, respectively. The heat flux due to radiation and CX is estimated to be about 2 W/cm^2. The scatter in the calculated heat flux is attributed to the statistical error due to the number of test particles (36000); this error is 10% at the heat flux peak. In the toroidal distribution [Fig. 6(a)], both profiles are similar but the measured flux spot appears at a lower toroidal angle than the calculated one. The toroidal angle asymmetry in the OFMC heat flux is due to the structure of magnetic field lines. In the experiments, the deepest ripple well is located at a toroidal angle of slightly more than 10°. In the poloidal distribution [Fig. 6(b)], the shape of both profiles is also similar. The ripple-trapped loss from the experiment is estimated to be $(8.8 \pm 1.4)\%$, whereas that from the OFMC code is $(9.2 \pm 0.9)\%$. Furthermore, the OFMC calculation indicates that an additional ripple loss of 13% due to collisional banana drift appears between PP 60 and 80 in this shot. Unfortunately, the banana drift loss has not

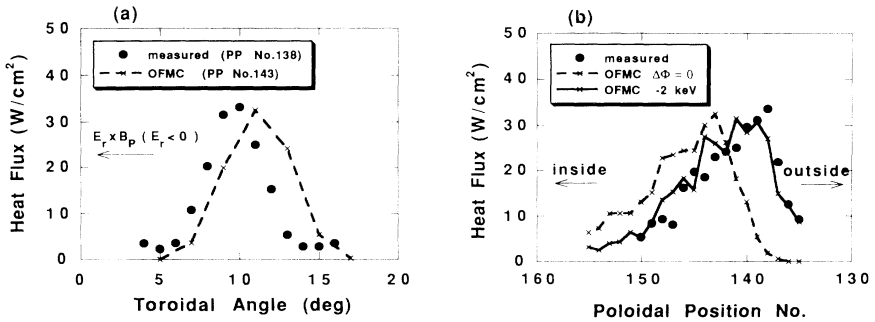

FIG. 6. Comparison between the measured and the calculated heat flux profiles: (a) the toroidal distribution and (b) the poloidal distribution. The experimental data are represented by solid circles. The calculated values are indicated by dashed lines ($\Delta\Phi = 0$) and a solid line ($\Delta\Phi = -2$ keV).

been identified so far because of the restricted viewing angle of the IRTV.

The only disagreement which can be seen in Fig. 6 is the slight difference in the heat spot position. The OFMC calculations performed for slightly different density and temperature profiles did not show a large change in the heat spot position. The most probable explanation for the disagreement is that the OFMC code does not include the radial electric field. Recently Itoh *et al.* [13] have pointed out that the radial electric field $\mathbf{E}_r$ affects the distribution of ripple-trapped loss particles on the first wall. The shift of the impinging point in the direction of the major radius ΔR due to $\mathbf{E}_r \times \mathbf{B}_T$ drift is approximately expressed by $\Delta R \approx Z\Delta\Phi R/W$, where Z, $\Delta\Phi$, R, and W are the charge number of the fast ions, the potential difference between the ripple-trapping position of fast ions and the first wall, the radial coordinate of the ripple-trapping position, and the energy of the fast ions, respectively. When $\mathbf{E}_r < 0$, which is the case of JT-60U with perpendicular NBI heating, the $\mathbf{E}_r \times \mathbf{B}_T$ drift shifts the impinging point outwards. The reconstructed poloidal heat flux with inclusion of $\Delta\Phi = -2$ keV is shown by a solid line in Fig. 6(b). Although there is no direct measurement available of the radial potential, $\Delta\Phi = -2$ keV is a good estimate, as determined from plasma rotation data. With inclusion of $\Delta\Phi$, the calculated heat flux agrees well with the experiment. The introduction of negative $\mathbf{E}_r$ can also explain the difference in the toroidal distribution [Fig. 6(a)]. The shift of the observed heat spot towards a low toroidal angle can be attributed to $\mathbf{E}_r \times \mathbf{B}_P$ drift. From the above considerations, we can conclude that the radial electric field should be included to predict the detailed heat deposition profile of ripple-lost particles on the first wall.

In conclusion, the measured heat load on the first wall due to fast-ion ripple loss was localized in both toroidal and poloidal directions. The heat deposition on the wall increased with both ripple size and safety factor. Aside from a small difference in the position of the heat spot, quantitative agreement between the experiments and the OFMC calculations was demonstrated. These results give the first experimental evidence that an OFMC calculation can predict fast-ion ripple loss quantitatively. The small difference between the experiments and the calculations in the heat spot position can be explained by the shift of the trajectories of the ripple-trapped ions in the radial electric field.

The authors gratefully thank Dr. S. Tsuji and Dr. M. Azumi for their help on MHD equilibrium analysis and the members of the JT-60 Team for their collaboration. A critical reading of the manuscript by Dr. S. W. Wolfe is appreciated.

---

[a]Present address: Kyushu University, Kasuga, Fukuoka, 816 Japan.

[1] O. A. Anderson and H. P. Furth, Nucl. Fusion **12**, 207 (1972).
[2] J. N. Davidson, Nucl. Fusion **16**, 731 (1976).
[3] K. C. Shaing and J. D. Callen, Nucl. Fusion **22**, 1061 (1982).
[4] S. D. Scott *et al.*, Nucl. Fusion **25**, 359 (1985).
[5] V. Basiuk *et al.*, in *Proceedings of the 1992 International Conference on Plasma Physics, Innsbruck* (European Physical Society, Petit-Lancy, Switzerland, 1992), Vol. 1, p. 175.
[6] G. Sadler *et al.*, in *Proceedings of the 1992 International Conference on Plasma Physics* (Ref. [5]), p. 167.
[7] K. Tobita *et al.*, in *Proceedings of the 1992 International Conference on Plasma Physics* (Ref. [5]), p. 171.
[8] R. J. Goldston, R. B. White, and A. H. Boozer, Phys. Rev. Lett. **47**, 647 (1981).
[9] R. Boivin, PPPL Report No. 2797, 1991 (to be published).
[10] S. Putvinskij *et al.*, Report No. ITER-IL-PH-1-9-1, 1989 (to be published).
[11] M. Tuszewski and J. P. Roubin, Nucl. Fusion **28**, 499 (1988).
[12] K. Tani, M. Azumi, H. Kishimoto, and S. Tamura, J. Phys. Soc. Jpn. **50**, 1726 (1981).
[13] K. Itoh, H. Sanuki, I.-S. Itoh, and K. Tani, Nucl. Fusion **31**, 1405 (1991).
[14] JT-60 Team, H. Ninomiya *et al.*, Phys. Fluids B **4**, 2070 (1992).

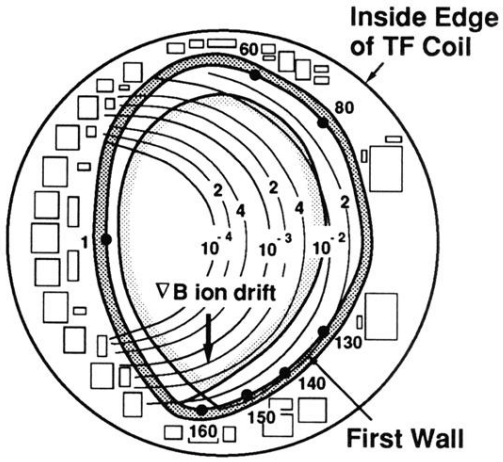

FIG. 1. Poloidal cross section of JT-60U plasma and the toroidal ripple distribution. Also shown are the poloidal position numbers of the first wall.

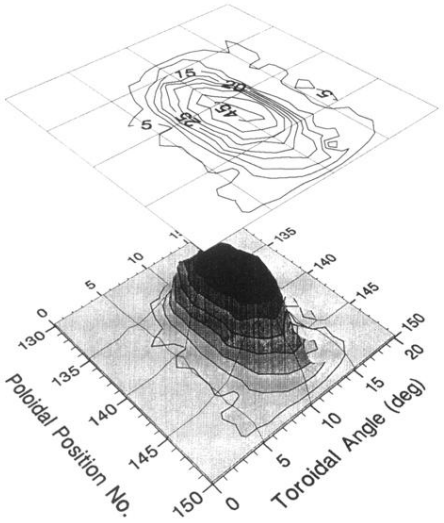

FIG. 2. Two-dimensional distribution of the heat deposition on the first wall. The TF coils are located at the toroidal angles of 0° and 20°. The heat flux peaks just between the TF coils. The magnitude of the heat flux is expressed in units of W/cm^2.

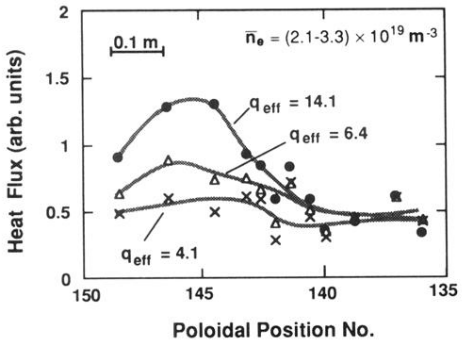

FIG. 4. The poloidal heat flux distribution for different values of q_{eff}. The heat deposition increases with q_{eff} because of the expansion of the ripple-trapping region.